

Article

Observing Femtosecond Fragmentation Using Ultrafast X-ray-Induced Auger Spectra

Thomas J. A. Wolf ¹ , Fabian Holzmeier ^{2,3}, Isabella Wagner ³, Nora Berrah ⁴, Christoph Bostedt ^{5,6,7}, John Bozek ^{2,5}, Phil Bucksbaum ^{1,8}, Ryan Coffee ⁵, James Cryan ¹, Joe Farrell ¹, Raimund Feifel ⁹, Todd J. Martinez ^{1,10} , Brian McFarland ¹, Melanie Mucke ¹¹, Saikat Nandi ^{2,12}, Francesco Tarantelli ¹³ , Ingo Fischer ³  and Markus Gühr ^{1,14,*}

¹ Stanford PULSE Institute, SLAC National Accelerator Laboratory, 2575 Sand Hill Road, Menlo Park, CA 94025, USA; thomas.wolf@stanford.edu (T.J.A.W.); phbuck@stanford.edu (P.B.); jcryan@slac.stanford.edu (J.C.); joepfar@gmail.com (J.F.); todd.martinez@stanford.edu (T.J.M.); bigbmac@gmail.com (B.M.)

² Synchrotron SOLEIL, L'Orme des Merisiers, Saint-Aubin, BP 48, 91192 Gif-sur-Yvette Cedex, France; fabian.holzmeier@synchrotron-soleil.fr (F.H.); john.bozek@synchrotron-soleil.fr (J.B.); saikat.nandi@fysik.lth.se (S.N.)

³ Institut für Physikalische & Theoretische Chemie, Universität Würzburg, D-97074 Würzburg, Germany; isabella.wagner@stud-mail.uni-wuerzburg.de (I.W.); ingo.fischer@uni-wuerzburg.de (I.F.)

⁴ Department of Physics, University of Connecticut, 2152 Hillside Road, Storrs, CT 06269, USA; nora.berrah@wmich.edu

⁵ Linac Coherent Light Source, SLAC National Accelerator Laboratory, 2575 Sand Hill Road, Menlo Park, CA 94720, USA; cbostedt@anl.gov (C.B.); coffee@slac.stanford.edu (R.C.)

⁶ Argonne National Laboratory, 9700 Cass Ave, Lemont, IL 60439, USA

⁷ Department of Physics and Astronomy, 2145 Sheridan Road, Northwestern University, Evanston, IL 60208, USA

⁸ Departments of Physics and Applied Physics, Stanford University, 382 Via Pueblo Mall, Stanford, CA 94305, USA

⁹ Department of Physics, University of Gothenburg, SE-412 96 Gothenburg, Sweden; raimund.feifel@physics.gu.se

¹⁰ Department of Chemistry, Stanford University, 333 Campus Drive, Stanford, CA 94305, USA

¹¹ Department of Physics and Astronomy, Uppsala University, Box 516, SE-751 20 Uppsala, Sweden; melanie.mucke@physics.uu.se

¹² Department of Physics, Lund University, P. O. Box 118, SE-221 00 Lund, Sweden

¹³ Department of Chemistry, Biology and Biotechnology, University of Perugia, 06123 Perugia, Italy; francesco.tarantelli@unipg.it

¹⁴ Institut für Physik und Astronomie, Universität Potsdam, 14476 Potsdam, Germany

* Correspondence: mguehr@uni-potsdam.de; Tel.: + 49-331-977-5571

Academic Editor: Kiyoshi Ueda

Received: 11 June 2017; Accepted: 28 June 2017; Published: 1 July 2017

Abstract: Molecules often fragment after photoionization in the gas phase. Usually, this process can only be investigated spectroscopically as long as there exists electron correlation between the photofragments. Important parameters, like their kinetic energy after separation, cannot be investigated. We are reporting on a femtosecond time-resolved Auger electron spectroscopy study concerning the photofragmentation dynamics of thymine. We observe the appearance of clearly distinguishable signatures from thymine's neutral photofragment isocyanic acid. Furthermore, we observe a time-dependent shift of its spectrum, which we can attribute to the influence of the charged fragment on the Auger electron. This allows us to map our time-dependent dataset onto the fragmentation coordinate. The time dependence of the shift supports efficient transformation of the excess energy gained from photoionization into kinetic energy of the fragments. Our method is broadly applicable to the investigation of photofragmentation processes.

Keywords: ultrafast dynamics; Auger electron spectroscopy; photofragmentation; photochemistry

1. Introduction

The speed of a photoexcited chemical reaction is determined by gradients of potential energy surfaces and the mass of reaction products or precursors. Generally, the decisive steps—the making or breaking of chemical bonds—occur on a femtosecond timescale. Numerous experimental methods have been implemented to approach this topic. The development of femtosecond laser pulses brought an extreme wealth of ultrafast techniques to life, among them visible and ultraviolet pump-probe spectroscopy [1] and multidimensional spectroscopy [2]. For isolated molecules, photoelectron spectroscopy [3] and electron, as well as X-ray scattering [4–6], have developed as high fidelity tools that can be directly compared to highest level ab initio calculations on isolated molecular dynamics.

In this article, we focus on investigating a specific type of reaction, photoion fragmentation as it occurs in the presence of ionizing radiation in the upper atmosphere or in space [7]. Organic molecules can be photoionized by absorbing either one or multiple photons, which combined can overcome the ionization potential (typically on the order of 9 eV [8]). When sufficient energy is deposited in the molecule, it is placed on a cationic potential energy surface with repulsive character in at least one internal degree of freedom. Thus, the nuclei are sped up towards rapid bond dissociation and fragmentation by a steep gradient in the Franck–Condon region. The positive charge localizes on one of the fragments. Charged and neutral species separate with considerable velocity.

Due to strongly different ionization potentials in charged and neutral species, such a process can only be investigated by probing the parent photocation and the fragments with photon energies considerably beyond what is readily available from table-top laser systems in the vacuum ultraviolet and soft X-ray regime.

Short wavelength pulses in the femtosecond domain with unprecedented pulse energy became available with the advent of X-ray free electron lasers [9–12]. For isolated molecules, this allowed for X-ray scattering experiments in extremely diluted targets [13–15] as well as the development of spectroscopic methods in the soft X-ray domain [16–22]. Due to the deeply-bound core electrons, X-ray spectroscopy is element-, as well as site-, selective [23].

In the present study, we demonstrate that unique insight into ionic photofragmentation can be gained by probing the dynamics using Auger electron spectroscopy. Here, the photoion and its fragments are core-ionized by a femtosecond soft X-ray pulse. They undergo Auger decay by filling the core hole with a valence electron and simultaneously ejecting another valence electron for energy conservation reasons, which is schematically shown in Figure 1. We measured the kinetic energy spectrum of the ejected Auger electron as a function of the time delay between the start of the photofragmentation reaction by the optical UV pulse and the X-ray ionization. By choosing the non-resonant soft X-ray photon energy to be high enough, Auger spectra of charged and neutral fragments can be observed simultaneously and the method is insensitive to small fluctuations of the photon energy at free electron lasers starting from noise. Furthermore, as shown in [16], Auger spectroscopy methods provide the unique opportunity to follow fragmentation dynamics beyond the typical bond distances of 1–2 Å, since molecular Auger decay channels, which involve valence electrons situated at different atoms, still function at considerably larger atomic distances. We show in the following that the Auger spectral features reveal signatures of fragmentation dynamics at even longer distances. This allows for determination of e.g., their kinetic energies and can, therefore, give important mechanistic information about the redistribution of energy during the fragmentation process.

We demonstrate the concept on a specific example, the multi-photon induced fragmentation process of the nucleobase thymine (see Figure 1). Ultraviolet light of 4.65 eV photon energy induces a resonant three photon transition to an excited ionic state, from where the molecule is predicted to fragment into neutral isocyanic acid (HNCO) and a charged C₄H₅NO⁺ fragment.

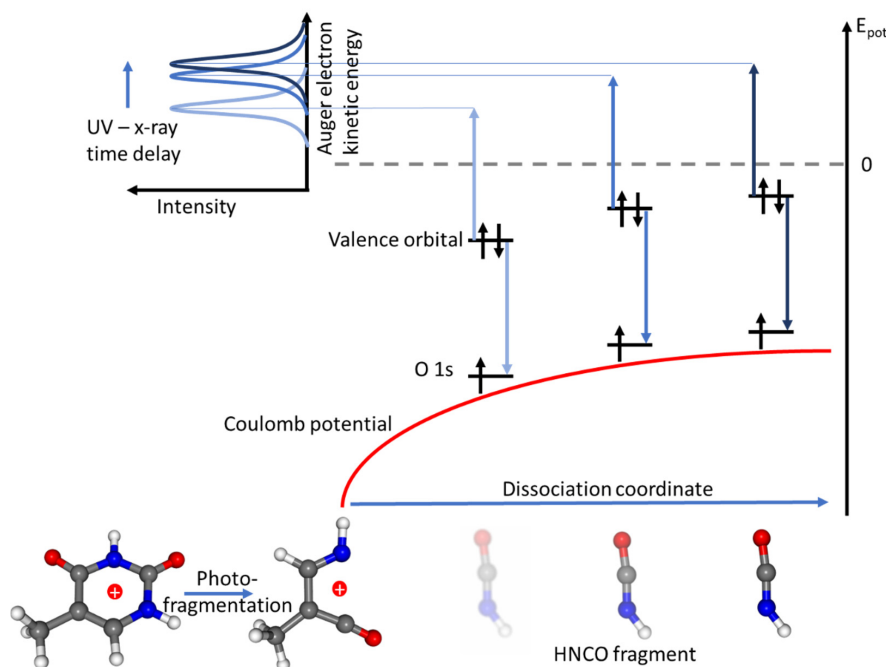


Figure 1. Probing molecular photofragmentation by soft X-ray-induced Auger spectra. We exemplify the method on the thymine molecular cation, which breaks apart into neutral isocyanic acid (HNCO) and singly-charged $C_4H_5NO^+$ after three-photon UV ionization (bottom). The distance of the HNCO fragment is interrogated by a time-delayed soft X-ray pulse creating core ionized molecules. The subsequent Auger decay leads to the emission of an additional electron, which does not only have to overcome the ionization potential intrinsic to the molecule, but also the external Coulomb potential (red) of the nearby cationic fragment. The Auger emission from the small neutral HNCO in the vicinity of the positively-charged large fragment leads to a red-shifted Auger kinetic energy with respect to the Auger electron spectrum of the isolated molecule. As the dissociation coordinate increases, the redshift asymptotically disappears.

Charged fragments have been observed in classical mass spectroscopy under high energy electron or photon excitation. The onset of the $C_4H_5NO^+$ fragment channel has been determined by threshold spectroscopy [24] to be above 10 eV. Thus, three photons of 4.65 eV photon energy need to be absorbed to observe the described fragmentation. The fragmentation of cationic thymine into HNCO and $C_4H_5NO^+$ has been theoretically investigated [25]. Although the reaction can be formally understood as a retro-Diels–Alder reaction, which should be concerted, a stepwise mechanism cleaving the two involved C–N bonds, as sketched in Figure 1, was found.

Large molecular systems possess a relatively unstructured Auger spectrum after creation of 1s core holes in carbon, nitrogen, or oxygen. Many different decay paths are energetically allowed and broad bands originating from the 2s2s, 2s2p, and 2p2p valence electron orbitals are involved in the Auger decay [17,26,27]. In terms of potential energy surfaces, one can rephrase this assertion by stating that the density of final states of the Auger decay process is high and the Auger lines overlap to form large bands.

After fragmentation and sufficient separation, however, electrons from the cationic fragment cannot take part in Auger decays on the neutral fragments, because such decay processes have distance dependences of r^{-6} [28]. Small molecules show relatively narrow lines with a width on the few 100 meV scale [29] because the density of final states is much lower as the number of electrons in the molecule is smaller. Different fragments can therefore be easily distinguished in the Auger spectra by characteristic sharp fingerprints. It is energetically more favorable to delocalize a positive charge on a large fragment than on a small one. Therefore, as a rule of thumb, neutral fragments will be observable as sharper

lines on top of a background from the cationic system with higher density of final states and, thus, less structural.

The electrons, which are emitted during Auger decay of the neutral fragment, still experience the Coulomb potential of the cationic fragment with considerably longer-range characteristic (r^{-1}) than the above mentioned joint neutral-charged fragment Auger channels (r^{-6}). The effect is observable by a shift of the Auger spectrum to lower kinetic energies.

Probing the fragmentation process just after the optical excitation still interrogates the large molecular ion. The Auger spectrum will be showing a broad unstructured band. After some time, however, fragmentation has taken place and one can treat the molecular fragments as small molecules with a reduced dicationic state density. The resulting spectrum will be structured in much sharper lines. These lines will first appear shifted with respect to their steady-state position (see Figure 1). The increasing distance of neutral and cationic fragments can then be followed in the reduction of this shift.

The article is structured in the following way: In the next section, we will introduce the experimental setups used at the free electron laser (FEL) and the synchrotron. The FEL setup was used to perform the time resolved dissociation experiment on the nucleobase thymine. Since the theoretically proposed fragmentation paths suggest splitting off neutral isocyanic acid (HNCO), we separately measured its Auger spectrum at a synchrotron to assign the neutral fragment.

We show the results and discuss spectral shape, as well as the spectral position of the fragment Auger lines. From the latter, we calibrate the distances of the fragments on a sub-picosecond timescale. We validate our calibration with a simple mechanical model based on full transformation of excess energy into the kinetic energy of the fragments.

2. Experimental Methods and Theory

The time-resolved fragmentation experiments on thymine were performed at the AMO (Atomic, Molecular and Optical physics) instrument of the LCLS (Linac Coherent Light Source) free electron laser. The instrument and some of its science are described in detail in [30,31]. Details of the setup we used for this particular experiment can be found in [17,32]. A sketch of the most important parts is given in Figure 2a. In short, thymine powder was evaporated in an oven at 140 °C with an outlet to the interaction region in the form of a heated capillary, thus forming an effusive jet in the collection volume of a magnetic bottle electron spectrometer.

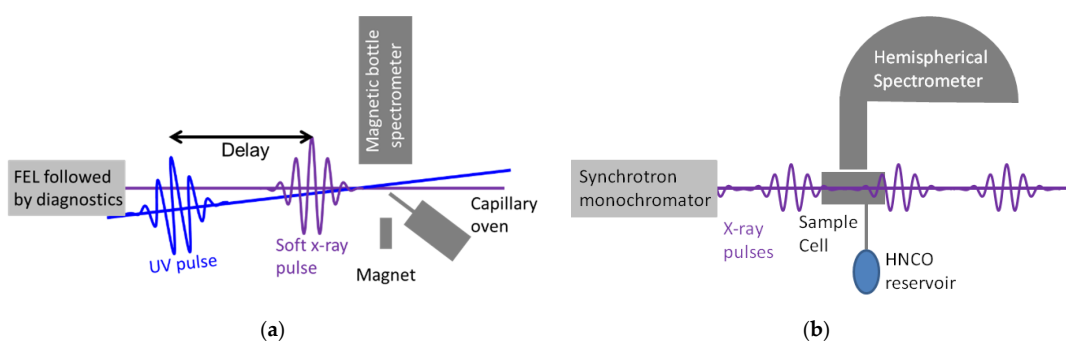


Figure 2. Experimental setups. (a) Sketch of the setup at the free electron laser. Molecules are inserted into the interaction region by evaporation in a capillary oven. A first UV pulse ionizes and fragments the molecules. The fragments are then probed by a delayed soft X-ray pulse via core electron ionization. The Auger electrons are collected and analyzed in a magnetic bottle spectrometer. (b) Sketch of the setup at the synchrotron beamline. Isocyanic acid is produced close to the beamline and then transported to the spectrometer under cryogenic conditions. The sample is inserted in a differentially pumped cell. Soft X-ray radiation from the monochromator beamline core ionizes the molecules and Auger electrons of HNCO are analyzed via a hemispherical electron analyzer.

A first UV pulse ($h\nu = 4.65$ eV, 70 fs duration) triggered the fragmentation process via resonance-enhanced three-photon ionization. A time-delayed free electron laser (FEL) soft X-ray pulse ($h\nu = 570$ eV, 70 fs duration) was used to create an oxygen core hole in the photoionized molecules. Auger electrons from O 1s core holes were detected with the magnetic bottle spectrometer as a function of time delay between UV excitation and X-ray probe pulses.

The time resolution of the experiment is about 330 fs, which is dominated by the jitter between the optical excitation and the FEL probe pulses. This is much larger than the time resolution observed in our study of the non-adiabatic dynamics in the neutral excited states of thymine [17], since we had not implemented the single shot optical X-ray cross-correlator [33] to compensate for the jitter between optical and FEL pulses in the data analysis for the fragmentation study reported here.

The steady state experiments on isolated HNCO were performed at the high-resolution photoelectron spectroscopy instrument of the PLEIADES beamline at the synchrotron SOLEIL [34]. A schematic overview is given in Figure 2b. Synchrotron light at a photon energy of $h\nu = 570$ eV and a bandwidth of 750 meV ionized the HNCO molecules contained in a differentially-pumped sample cell with entrance and exit windows for the synchrotron beam. The emitted O 1s Auger electrons in the direction of the light polarization were dispersed by a hemispherical analyzer. The monochromator, as well as the hemispherical analyzer were calibrated by measuring the photoabsorption and Auger spectra of CO₂.

The isocyanic acid target was prepared according to the method described in [35]. After synthesis, the molecular sample was stored at liquid nitrogen temperatures to avoid polymerization. The vapor pressure at around -40 °C was sufficient to obtain the necessary molecular density inside the gas cell attached to the hemispherical analyzer.

The O1s core decay spectrum of HNCO has been calculated using the second-order Algebraic Diagrammatic Construction (ADC(2)), which is a well-established Green's function-based direct method to compute double ionization and Auger spectra [36,37] in combination with a cc-pVDZ basis [38]. The details of the simulation are described in [17].

3. Results and Discussion

Figure 3a shows Auger spectra of fragmenting thymine ions as a function of kinetic energy. The different spectra are measured at various time delays between the UV ionization and X-ray probe pulse as given in the figure. At negative delays, the ultra-short X-ray pulses hit molecules before the ultraviolet photoionization, thus, those spectra reflect the core hole decay of thymine in its electronic ground state. The spectrum is only weakly structured, centered around 504 eV photon energy, and possesses a width of around 10 eV. The Auger spectra of thymine have been published by us in another context, however, we realized during the work on this publication, that the energy calibration in [17] must be shifted up by 3 eV. The ADC(2) theory in [17] was too high in energy by about 1.5 eV; now it is too low compared to the experimental thymine spectrum by about the same amount.

The overlap of UV and X-ray pulses in the pump-probe experiment manifests itself by a strong bleach of the main Auger line due to the removal of the population from the electronic ground state of neutral thymine [17]. This feature has also been used to set the zero-delay time for this experiment. As shown in Figure 3a, the Auger spectrum broadens considerably and develops a pronounced wing towards lower kinetic energies after the UV pulse excitation. The underlying reason for this wing are additional states newly populated by absorption of the UV pump pulse. In part, this is the desired, dissociative cationic state. Since the photoionization efficiency is enhanced by resonant excited states in the neutral molecule, there are certainly additional contributions from population in those states. From our previous study [17], we know that photoexcitation to the lowest valence state of the neutral results in a shift of the Auger spectrum to lower energies by about 5 eV within 500 fs. We can expect the Auger electron spectrum of the cationic state to shift more strongly in the same direction, simply based on the argument that Auger electron emission must work against one more charge in the molecular ion compared to the case of Auger decay from a core-ionized neutral molecule. The combination of energy

shifts to the spectrum from excited and ionized states can explain unambiguously the appearance of a broad signature at lower electron kinetic energies.

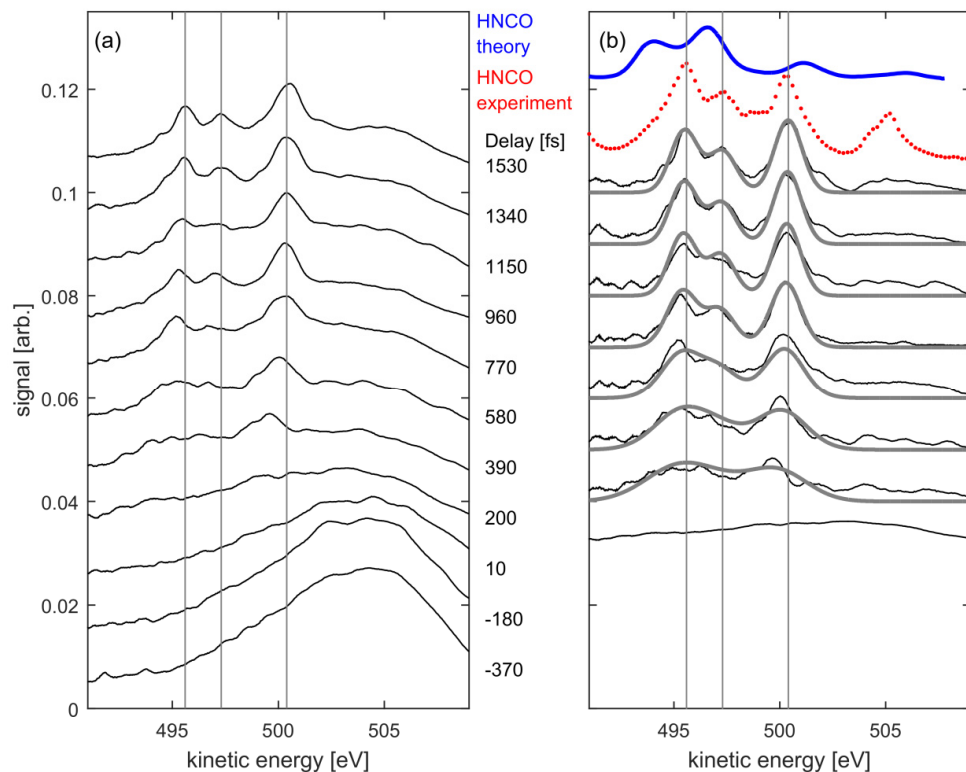


Figure 3. Results of the transient Auger studies on fragmenting thymine ions. **(a)** The Auger spectra of the UV-fragmented molecules are shown as a function of delay between the UV and soft X-ray pulse. Narrow lines appear on a broadening baseline with increasing delay. The three vertical grey lines indicate the position of peak maxima for long delays, showing that the narrow lines shift towards higher energies with increasing delay. The time-resolved data is synthesized from single FEL shots. The relative error of the spectral intensity is on the order of 5–10%, which was determined in another paper on data from the same lincac coherent light source experiment using bootstrap statistical analysis [17]. **(b)** The same transient spectra as in **(a)**, corrected by a background (see text). For large delays, the transient spectrum fits the reference HNCO spectrum taken at the synchrotron (red dots). The relative intensity error in the significant range is on the order of a few percent. The calculation indicated in blue reproduces all the essential features of the HNCO reference spectrum, although with slightly different peak distances. The thick grey lines model the transient spectra by shifting and broadening three Gaussian lines according to a one-dimensional fragmentation process as described in the text.

Two new features, having a width smaller than the broad underlying band, appear in the spectrum after about 400 fs. At a UV-X-ray delay of 600 fs, three features stand out in the lower kinetic energy wing. They continue to sharpen and shift towards higher kinetic energies as the delay progresses. At 1200 fs after UV excitation, the features have reached a steady state.

We now compare the time-resolved spectra with steady-state Auger spectra of HNCO. The red dotted line in Figure 3b is the steady-state spectrum of HNCO as taken at the PLEIADES beamline of SOLEIL. The spectrum is characterized by 4 dominant peaks in the region between 494 and 508 eV. To further understand the character of these signatures, we also calculated the Auger decay features using the ADC(2) method. The method has been described in the context of thymine in [17]. The result of the calculation is shown as the solid blue spectrum on top of Figure 3b. The simulation reproduces the essential features of the steady-state experimental spectrum. The four lower energy maxima are

reproduced by the ADC(2) calculation. The upper energy maximum is only poorly modulated in the simulation. In addition, we observe energy shifts in the four lower maxima. Shifts on the order of 1 eV are typical for the ADC(2) method and the deviations will be the topic of future investigations.

In order to discern the details of the sharp features in the time-resolved spectra we model a background from a scaled spectrum at a 200 fs delay and subtract it from the spectra at all delays. The scaling factor is fitted such that the low and high energy wings of the spectra after this delay essentially have zero background. We plot the background-corrected spectra in Figure 3b. The Auger spectra of UV-photoionized thymine for delays 1150, 1340, and 1530 fs show a very good agreement with the steady-state Auger spectrum of HNCO. The three lower peaks at positions of 495.6, 497.3 and 500.4 eV (in the remainder of the paper labeled as Peak 1–3 in ascending Auger electron kinetic energy) are perfectly reproduced both in position and width. The highest energy peak at 505.2 eV in the steady-state spectrum is not well reproduced in the time-dependent spectra. This can be attributed to additional contributions from excited state dynamics in the neutral thymine and the ground state bleach, which are known to both appear in this regime [17]. Inspecting the transient trend in these peaks, one realizes that the peak width as well as position follows a similar trend for all three features. The peaks sharpen after the UV excitation to reach their stationary shape at about 1 ps. In addition, all peaks experience a shift towards higher kinetic energies. Around 400 fs, peak 3 appears at 499.7 eV, which is 0.7 eV shifted from the steady state. Around 770 fs, this shift diminishes to 0.3 eV. At the same delay, peak 1 is also red-shifted by about 0.3 eV from its steady state value of 495.6 eV. Peak 2 needs a longer time to fully form and also has a larger shift than the high and low energy features. At 770 fs, it is shifted by 0.6 eV lower from the steady state value of 497.3 eV.

In the following, we provide an explanation of the three main observations in the experimental data, the appearance of sharp new features, their spectroscopic shift, and their sharpening. From our calculations of the Auger spectra of thymine, we know that both oxygen atoms of thymine give rise to very dense spectral features, resulting from the high density of final states (DOFS) in this rather large molecule [17]. The high DOFS is reflected in a broad and unstructured Auger spectrum even for only one of the two oxygen atoms, demonstrated by calculations in the supporting material in [17]. From photoion mass spectrometry, it was suggested that photoionized thymine fragments into neutral HNCO and a positively-charged residual with mass 83 [24]. As the neutral HNCO fragment splits off the positively-charged residual, the electronic overlap between the two constituents gets smaller. This in turn reduces the density of dicationic states, in particular for the small HNCO fragment with only 22 electrons compared to the 43 electrons of the $C_4H_5NO^+$ fragment. The appearance of narrow lines within 600 fs, therefore, directly reflects the formation of neutral HNCO fragments.

The transient shift in the peak positions stems from the interaction of the outgoing Auger electron of HNCO with the positive charge of the $C_4H_5NO^+$ fragment. If the Auger electron is emitted in the vicinity of a positive fragment, it has to overcome the Coulomb potential of that charge. It is, thus, detected with lower kinetic energy compared to a HNCO Auger electron being emitted far away from the charged fragment. With the assumption of the Coulomb interaction resulting in a shift in atomic units being directly 1/distance to be responsible for the peak shifts, we can directly determine distances between charged and neutral fragments from the energy shifts. The distances are listed in Table 1. The evaluated distances for different peaks in part differ considerably, which can be mainly attributed to the limited accuracy to which the peak positions could be extracted from the spectra.

Table 1. Fragment distances calculated based on the transient peak shifts in the Auger electron spectra and a Coulomb interaction. The confidence intervals are calculated assuming a constant error in relative peak position of 0.1 eV. For comparison, the expected distances under the model assumption of one-dimensional fragmentation that the entire absorbed excess energy is transformed into kinetic energy are included.

Delay (fs)	Peak 1, Distance (Å)	Peak 2, Distance (Å)	Peak 3, Distance (Å)	Model, Distance (Å)
380	-	-	21 ± 3	17
580	-	-	36 ± 9	27
770	48 ± 16	24 ± 4	48 ± 16	35
960	72 ± 36	72 ± 36	144 ± 144	44

We confirm the validity of our interpretation by comparing the values in Table 1 with time-dependent distances calculated under the model assumption that the entire excess energy from the UV photoionization is transferred into kinetic energy. It is clear that three UV photons of 4.65 eV are needed to overcome the appearance energy of 10.7 eV for HNCO fragments in thymine [24]. This leaves approximately 3 eV of excess kinetic energy. The masses of HNCO and the C₄H₅NO⁺ fragment are $m_1 = 43$ a.u. and $m_2 = 83$ a.u., respectively, and the velocity of their separation approximately 4600 m/s. The distance of the two fragments x as a function of time t is given in Equation (1):

$$x(t) = v_2 t + v_1 t = t \left(\sqrt{\frac{2E_{kin}}{m_2 \left(\frac{m_2}{m_1} + 1 \right)}} + \sqrt{\frac{2E_{kin}}{m_1 \left(\frac{m_1}{m_2} + 1 \right)}} \right) \quad (1)$$

Time-dependent distances from this model agree reasonably well with those from evaluating the peak shifts, which strongly supports our assignment to the effect of Coulomb interactions with the cationic fragment.

We are using the expression for time-dependent distances to model the evolution of the HNCO Auger spectra. We are describing the HNCO peaks as Gaussian functions with 1.5 eV full width at half maximum as extracted from the steady-state HNCO spectra. We simulate the time-dependent shifts by assuming a pure Coulombic 1/x potential (using atomic units). A trivial explanation for the peak sharpening would be that it is due to the limited time resolution of 330 fs. Since the gradient of the Coulomb potential has an inverse dependence on the distance to the charged fragment, sampling over the 330 fs time evolution would broaden the peaks more strongly at earlier times than at later times. Convoluting our modeled time-dependent spectra, however, does not completely account for the peak sharpening. To achieve good agreement with experimental spectra, we had to include an additional time-dependent broadening to the Gaussian functions, which decreases from 4.7 to 1.5 eV during the first picosecond. The Gaussian peaks are normalized according to their area and scaled by the same universal factor for all time delays. The resulting simulated spectra are given as the grey thick lines in Figure 3b. The shift as well as the position fits well within the noise on the experimental Auger spectra.

The additional broadening most likely stems from the finite width of the nuclear wavepacket. From [24], we know that the dissociating nuclear wavepacket has to overcome two potential barriers which will broaden it in the dissociation coordinate. The broad wavepacket in this degree of freedom will have a similar effect as the time resolution on the Auger electron peak width. At small distances/early times, there might, however, be an additional contribution from long-range interactions during Auger decay, which can have a distance-dependent effect on the DOFS, even at separations of several angstroms substantially beyond the van der Waals radii [16]. Future experiments with improved time resolution can easily investigate this early phase of photofragmentation. This should allow us to follow the reduction in DOFS during separation of the fragments in real-time and provide important information about the nature of the fragmentation process.

4. Conclusions

We conclude by pointing out the unique long-range sensitivity of Auger electron spectroscopy to the presence of charged particles, which allows one to map time-dependent signatures of fragments onto a dissociation coordinate. The important observable, the spectral shift with respect to field-free Auger decay, can be easily interpreted based on a Coulomb potential without recourse to more complicated theory. In principle, any probe process generating and detecting charged particles is sensitive to the Coulomb potential of a nearby charged fragment. However, the sensitivity is strongly reduced in the case of ion detection due to their orders of magnitude larger masses. Valence electron spectroscopy should, in principle, show the same effect. However, due to strong vibrational substructure in valence photoelectron spectra, the effect would be difficult to observe, Auger electron spectroscopy on the other hand has the dynamic range to observe both the signatures of the molecular ground state and of the fragmentation process. Moreover, due to the strong difference in DOFS, it provides distinct signatures of fragment generation. Future experiments are planned to exploit this powerful X-ray induced Auger electron technique.

Acknowledgments: This work was supported by the AMOS program within the Chemical Sciences, Geosciences, and Biosciences Division of the Office of Basic Energy Sciences, Office of Science, U.S. Department of Energy. Parts of this research were carried out at the Linac Coherent Light Source (LCLS) at the SLAC National Accelerator Laboratory. LCLS is an Office of Science User Facility operated for the U.S. Department of Energy Office of Science by Stanford University. Parts of this research were carried out at the PLEIADES beamline, Soleil Synchrotron, France. MG acknowledges funding via the Office of Science Early Career Research Program through the Office of Basic Energy Sciences, U.S. Department of Energy and NB under grant no. DE-SC0012376. MG is funded by a Lichtenberg Professorship from the Volkswagen foundation. IF acknowledges DFG, Project FI 575/7-3 for funding. TJA W thanks the German National Academy of Sciences Leopoldina for a fellowship (Grant No. LPDS2013-14). R.F. acknowledges funding from the Swedish Research Council (VR), the Göran Gustafsson Foundation and the Knut and Alice Wallenberg Foundation, Sweden. We thank S. Miyabe, A. Aguilar, J. C. Castagna, L. Fang, J. M. Glownia, B. Murphy, A. Natan, T. Osipov, V. S. Petrovic, S. Schorb, T. Schultz, L. S. Spector, M. Swiggers, I. Tenney, S. Wang, and J. L. White for contributions to the thymine experimental data.

Author Contributions: Markus Gühr, Nora Berrah, Christoph Bostedt, John Bozek, Phil Bucksbaum, Ryan Coffee, James Cryan, Joseph Farrell, Raimund Feifel, Todd J. Martinez, Brian McFarland, and Melanie Mucke prepared and conducted the time-resolved experiment at LCLS and analyzed the results. Thomas J. A. Wolf, Fabian Holzmeier, Isabella Wagner, Saikat Nandi, Ingo Fischer, and Markus Gühr synthesized HINCO and performed the experiment at Synchrotron Soleil. Francesco Tarantelli performed the simulations. Markus Gühr analyzed the experimental data. Thomas J. A. Wolf, Markus Gühr, Fabian Holzmeier, and Ingo Fischer analyzed the results and wrote the paper.

Conflicts of Interest: The authors declare no conflict of interest.

References

1. Zewail, A.H. Femtochemistry: Atomic-Scale Dynamics of the Chemical Bond Using Ultrafast Lasers (Nobel Lecture). *Angew. Chem. Int. Ed.* **2000**, *39*, 2586–2631. [[CrossRef](#)]
2. Mukamel, S. *Principles of nonlinear optical spectroscopy*; Oxford university press: Oxford, UK, 1995.
3. Blanchet, V.; Zgierski, M.Z.; Seideman, T.; Stolow, A. Discerning vibronic molecular dynamics using time-resolved photoelectron spectroscopy. *Nature* **1999**, *401*, 52–54. [[CrossRef](#)]
4. Srinivasan, R.; Lobastov, V.A.; Ruan, C.-Y.; Zewail, A.H. Ultrafast Electron Diffraction (UED). *Helv. Chim. Acta* **2003**, *86*, 1761–1799. [[CrossRef](#)]
5. Yang, J.; Guehr, M.; Vecchione, T.; Robinson, M.S.; Li, R.; Hartmann, N.; Shen, X.; Coffee, R.; Corbett, J.; Fry, A.; et al. Diffractive imaging of a rotational wavepacket in nitrogen molecules with femtosecond megaelectronvolt electron pulses. *Nat. Commun.* **2016**, *7*, 11232. [[CrossRef](#)] [[PubMed](#)]
6. Yang, J.; Guehr, M.; Shen, X.; Li, R.; Vecchione, T.; Coffee, R.; Corbett, J.; Fry, A.; Hartmann, N.; Hast, C.; et al. Diffractive Imaging of Coherent Nuclear Motion in Isolated Molecules. *Phys. Rev. Lett.* **2016**, *117*, 153002. [[CrossRef](#)] [[PubMed](#)]
7. Dishoeck, E.F. Astrochemistry of dust, ice and gas: introduction and overview. *Faraday Discuss.* **2014**, *168*, 9–47. [[CrossRef](#)] [[PubMed](#)]
8. Koch, M.; Wolf, T.J.A.; Gühr, M. Understanding the modulation mechanism in resonance-enhanced multiphoton probing of molecular dynamics. *Phys. Rev. A* **2015**, *91*, 031403. [[CrossRef](#)]

9. Ackermann, W.; Asova, G.; Ayvazyan, V.; Azima, A.; Baboi, N.; Bähr, J.; Balandin, V.; Beutner, B.; Brandt, A.; Bolzmann, A.; et al. Operation of a free-electron laser from the extreme ultraviolet to the water window. *Nat. Photonics* **2007**, *1*, 336–342. [[CrossRef](#)]
10. Emma, P.; Akre, R.; Arthur, J.; Bionta, R.; Bostedt, C.; Bozek, J.; Brachmann, A.; Bucksbaum, P.; Coffee, R.; Decker, F.-J.; et al. First lasing and operation of an angstrom-wavelength free-electron laser. *Nat. Photonics* **2010**, *4*, 641–647. [[CrossRef](#)]
11. Ishikawa, T.; Aoyagi, H.; Asaka, T.; Asano, Y.; Azumi, N.; Bizen, T.; Ego, H.; Fukami, K.; Fukui, T.; Furukawa, Y.; et al. A compact X-ray free-electron laser emitting in the sub-ångström region. *Nat. Photonics* **2012**, *6*, 540–544. [[CrossRef](#)]
12. Allaria, E.; Appio, R.; Badano, L.; Barletta, W.A.; Bassanese, S.; Biedron, S.G.; Borga, A.; Busetto, E.; Castronovo, D.; Cinquegrana, P.; et al. Highly coherent and stable pulses from the FERMI seeded free-electron laser in the extreme ultraviolet. *Nat. Photonics* **2012**, *6*, 699–704. [[CrossRef](#)]
13. Minitti, M.P.; Budarz, J.M.; Kirrander, A.; Robinson, J.S.; Ratner, D.; Lane, T.J.; Zhu, D.; Glownia, J.M.; Kozina, M.; Lemke, H.T.; et al. Imaging Molecular Motion: Femtosecond X-Ray Scattering of an Electrocyclic Chemical Reaction. *Phys. Rev. Lett.* **2015**, *114*, 255501. [[CrossRef](#)] [[PubMed](#)]
14. Küpper, J.; Stern, S.; Holmegaard, L.; Filsinger, F.; Rouzée, A.; Rudenko, A.; Johnsson, P.; Martin, A.V.; Adolph, M.; Aquila, A.; et al. X-Ray Diffraction from Isolated and Strongly Aligned Gas-Phase Molecules with a Free-Electron Laser. *Phys. Rev. Lett.* **2014**, *112*, 083002. [[CrossRef](#)]
15. Glownia, J.M.; Natan, A.; Cryan, J.P.; Hartsock, R.; Kozina, M.; Minitti, M.P.; Nelson, S.; Robinson, J.; Sato, T.; van Driel, T.; et al. Self-Referenced Coherent Diffraction X-Ray Movie of Ångstrom and Femtosecond-Scale Atomic Motion. *Phys. Rev. Lett.* **2016**, *117*, 153002. [[CrossRef](#)] [[PubMed](#)]
16. Erk, B.; Boll, R.; Trippel, S.; Anielski, D.; Foucar, L.; Rudek, B.; Epp, S.W.; Coffee, R.; Carron, S.; Schorb, S.; et al. Imaging charge transfer in iodomethane upon x-ray photoabsorption. *Science* **2014**, *345*, 288–291. [[CrossRef](#)] [[PubMed](#)]
17. McFarland, B.K.; Farrell, J.P.; Miyabe, S.; Tarantelli, F.; Aguilar, A.; Berrah, N.; Bostedt, C.; Bozek, J.D.; Bucksbaum, P.H.; Castagna, J.C.; et al. Ultrafast X-ray Auger probing of photoexcited molecular dynamics. *Nat. Commun.* **2014**, *5*, 4235. [[CrossRef](#)] [[PubMed](#)]
18. Liekhus-Schmaltz, C.E.; Tenney, I.; Osipov, T.; Sanchez-Gonzalez, A.; Berrah, N.; Boll, R.; Bomme, C.; Bostedt, C.; Bozek, J.D.; Carron, S.; et al. Ultrafast isomerization initiated by X-ray core ionization. *Nat. Commun.* **2015**, *6*, 8199. [[CrossRef](#)] [[PubMed](#)]
19. Petrovic, V.S.; Siano, M.; White, J.L.; Berrah, N.; Bostedt, C.; Bozek, J.D.; Broege, D.; Chalfin, M.; Coffee, R.N.; Cryan, J.; et al. Transient X-ray Fragmentation: Probing a Prototypical Photoinduced Ring Opening. *Phys. Rev. Lett.* **2012**, *108*, 253006. [[CrossRef](#)] [[PubMed](#)]
20. Berrah, N.; Fang, L.; Murphy, B.; Osipov, T.; Ueda, K.; Kukk, E.; Feifel, R.; van der Meulen, P.; Salen, P.; Schmidt, H.T.; et al. Double-core-hole spectroscopy for chemical analysis with an intense X-ray femtosecond laser. *Proc. Natl. Acad. Sci. U. S. A.* **2011**, *108*, 16912–16915. [[CrossRef](#)] [[PubMed](#)]
21. Wolf, T.J.A.; Myhre, R.H.; Cryan, J.P.; Coriani, S.; Squibb, R.J.; Battistoni, A.; Berrah, N.; Bostedt, C.; Bucksbaum, P.; Coslovich, G.; et al. Probing ultrafast $\pi\pi^*/n\pi^*$ internal conversion in organic chromophores via K-edge resonant absorption. *Nat. Commun.* **2017**, *8*, 29. [[CrossRef](#)] [[PubMed](#)]
22. Ullrich, J.; Rudenko, A.; Moshammer, R. Free-Electron Lasers: New Avenues in Molecular Physics and Photochemistry. *Annu. Rev. Phys. Chem.* **2012**, *63*, 635–660. [[CrossRef](#)] [[PubMed](#)]
23. Siegbahn, K. *ESCA Applied to Free Molecules*; North-Holland Pub. Co: Amsterdam, The Netherlands, 1969.
24. Jochims, H.-W.; Schwell, M.; Baumgärtel, H.; Leach, S. Photoion mass spectrometry of adenine, thymine and uracil in the 6–22 eV photon energy range. *Chem. Phys.* **2005**, *314*, 263–282. [[CrossRef](#)]
25. Improta, R.; Scalmani, G.; Barone, V. Radical cations of DNA bases: some insights on structure and fragmentation patterns by density functional methods. *Int. J. Mass Spectrom.* **2000**, *201*, 321–336. [[CrossRef](#)]
26. Storchi, L.; Tarantelli, F.; Veronesi, S.; Bolognesi, P.; Fainelli, E.; Avaldi, L. The Auger spectroscopy of pyrimidine and halogen-substituted pyrimidines. *J. Chem. Phys.* **2008**, *129*, 154309. [[CrossRef](#)] [[PubMed](#)]
27. Rennie, E.E.; Hergenhahn, U.; Kugeler, O. A core-level photoionization study of furan. *J. Chem. Phys.* **2002**, *117*, 6524–6532. [[CrossRef](#)]
28. Sisourat, N.; Kryzhevci, N.V.; Kolorenč, P.; Scheit, S.; Jahnke, T.; Cederbaum, L.S. Ultralong-range energy transfer by interatomic Coulombic decay in an extreme quantum system. *Nat. Phys.* **2010**, *6*, 508–511. [[CrossRef](#)]

29. Moddeman, W.E.; Carlson, T.A.; Krause, M.O.; Pullen, B.P.; Bull, W.E.; Schweitzer, G.K. Determination of the K-LL Auger Spectra of N₂, O₂, CO, NO, H₂O, and CO₂. *J. Chem. Phys.* **1971**, *55*, 2317–2336. [CrossRef]
30. Ferguson, K.R.; Bucher, M.; Bozek, J.D.; Carron, S.; Castagna, J.-C.; Coffee, R.; Curiel, G.I.; Holmes, M.; Krzywinski, J.; Messerschmidt, M.; et al. The Atomic, Molecular and Optical Science instrument at the Linac Coherent Light Source. *J. Synchrotron Radiat.* **2015**, *22*, 492–497. [CrossRef] [PubMed]
31. Bozek, J.D. AMO instrumentation for the LCLS X-ray FEL. *Eur. Phys. J.-Spec. Top.* **2009**, *169*, 129–132. [CrossRef]
32. McFarland, B.K.; Berrah, N.; Bostedt, C.; Bozek, J.; Bucksbaum, P.H.; Castagna, J.C.; Coffee, R.N.; Cryan, J.P.; Fang, L.; Farrell, J.P.; et al. Experimental strategies for optical pump: Soft X-ray probe experiments at the LCLS. *J. Phys. Conf. Ser.* **2014**, *488*, 12015. [CrossRef]
33. Schorb, S.; Gorkhover, T.; Cryan, J.P.; Glownia, J.M.; Bionta, M.R.; Coffee, R.N.; Erk, B.; Boll, R.; Schmidt, C.; Rolles, D.; et al. X-ray-optical cross-correlator for gas-phase experiments at the Linac Coherent Light Source free-electron laser. *Appl. Phys. Lett.* **2012**, *100*, 121107. [CrossRef]
34. Lindblad, A.; Söderström, J.; Nicolas, C.; Robert, E.; Miron, C. A multi-purpose source chamber at the PLEIADES beamline at SOLEIL for spectroscopic studies of isolated species: Cold molecules, clusters, and nanoparticles. *Rev. Sci. Instrum.* **2013**, *84*, 113105. [CrossRef] [PubMed]
35. Fischer, G.; Geith, J.; Klapötke, T.M.; Krumm, B. Synthesis, Properties and Dimerization Study of Isocyanic Acid. *Z. Für Naturforschung B* **2002**, *57*, 19–24. [CrossRef]
36. Schirmer, J.; Barth, A. Higher-order approximations for the particle-particle propagator. *Z. Phys. At. Nucl.* **1984**, *317*, 267–279. [CrossRef]
37. Tarantelli, F. The calculation of molecular double ionization spectra by Green's functions. *Chem. Phys.* **2006**, *329*, 11–21. [CrossRef]
38. Kendall, R.A.; Dunning, T.H.; Harrison, R.J. Electron affinities of the first-row atoms revisited. Systematic basis sets and wave functions. *J. Chem. Phys.* **1992**, *96*, 6796–6806. [CrossRef]



© 2017 by the authors. Licensee MDPI, Basel, Switzerland. This article is an open access article distributed under the terms and conditions of the Creative Commons Attribution (CC BY) license (<http://creativecommons.org/licenses/by/4.0/>).